JOURNAL OF SOLID STATE CHEMISTRY 57, 166–177 (1985)

Zr-Doped Na_3PO_4: Crystal Chemistry, Phase Relations, and Polymorphism

S. J. MILNE AND A. R. WEST

University of Aberdeen, Department of Chemistry, Meston Walk, Old Aberdeen AB9 2UE, United Kingdom

Received June 6, 1984

Na_3PO_4 forms an extensive range of solid solutions with the replacement mechanism $4Na^+ \rightleftharpoons Zr^{4+}$ and formula, $Na_{9-4y}Zr_y(PO_4)_3$. The solid solution limit is $y \simeq 0.50$ below ~800°C, increasing to $y \sim 0.56$ by 1150°C. The high-temperature solid solutions have the cubic γ-Na_3PO_4 structure. At lower temperatures, various ordering reactions occur with increasing y. For $0.125 \lesssim y \lesssim 0.40$, the γ_{ord} phase forms with a cubic supercell, eight times the volume of the subcell. For $y \gtrsim 0.40$, the δ,δ' phases form which are characterized by line splitting and extra weak lines in the X-ray powder patterns, respectively. The γ_{ord} phase has a domain structure in which the domains decrease in size with both decreasing y and increasing temperature. A model for the formation of the γ_{ord} phase is proposed based on ordering of Zr^{4+} ions in alternate cubic subcells. The phase diagram for the orthophosphate join Na_3PO_4–$NaZr_2(PO_4)_3$ is presented.

Introduction

During a study of compound formation and conductivity in the Nasicon precursor system, Na_2O–P_2O_5–ZrO_2, a new, zirconium-doped, Na_3PO_4 solid solution series was discovered (*1*). These solid solutions have the formula, $Na_{3-4x}Zr_xPO_4$, $0 < x \lesssim 0.19$, at 1150°C. Their conductivity was measured (*2*) and found to pass through a maximum at compositions near $x = 0.13$ with a value of 2.5×10^{-2} ohm^{-1} cm^{-1} at 300°C. This value is less than one order of magnitude smaller than that of Nasicon or β-alumina at 300°C; consequently, the new materials may have possible applications in high-temperature cells.

Na_3PO_4 is polymorphic. It undergoes a reversible transition, α (tetragonal) to γ (cubic) at ~330°C. The α form has unit cell dimensions $a = 10.81$, $c = 6.84$ Å (*3*) although its structure is, as yet, unknown. The γ form has unit cell dimension, $a = 7.512$ Å, space group $Fm3m$, at 400°C, and its structure was solved by powder neutron diffraction (*4*). It may be regarded as a cation excess antifluorite structure with orientational disorder of the PO_4^{3-} groups. The existence of a third polymorph, β, has been proposed (*5*) as an intermediate in the $\alpha \rightleftharpoons \gamma$ transition. It is orthorhombic, $a = 6.963$, $b = 11.047$, $c = 5.562$ Å. It was also suggested (*5*) that the γ polymorph is only pseudocubic and that its true symmetry is orthorhombic with $a = 5.237$, $b = 5.203$, $c = 7.400$ Å.

The effect of additives on the polymorphism of Na_3PO_4 has been studied. The cations Ca^{2+}, Sr^{2+}, Cd^{2+}, Zn^{2+} (*6*), and Al^{3+} (*3*) enter the structure and lead to stabilization

0022-4596/85 $3.00

of the cubic γ polymorph at room temperature. Low-temperature ordering phenomena have been observed in several of these systems (*6*): with added Ca^{2+} or Sr^{2+}, an ordered tetragonal phase was reported, a = 14.860, c = 14.076 Å, whose unit cell volume is essentially eight times as large as that of the cubic γ phase. The crystal structure of the cubic, Al-stabilized γ polymorph has been studied (*7*). Na_3PO_4 is hygroscopic and forms several hydrate phases: $Na_3PO_4 \cdot xH_2O$ including x = 0.5, 8, and 12 (*8–10*).

This paper reports on the Zr-doped Na_3PO_4 solid solution system. The polymorphism, crystal chemistry, and thermal stability of the solid solutions has been studied. Anomalies in the polymorphism of Na_3PO_4 have been clarified. A detailed study of order–disorder phenomena in the Na_3PO_4 solid solutions has been made and the phase diagram of the pseudobinary, orthophosphate join, Na_3PO_4–$NaZr_2P_3O_{12}$, determined. Part of this phase diagram, extending from the Nasicon end member $NaZr_2P_3O_{12}$ to $Na_5ZrP_3O_{12}$ was reported previously (*12, 13*).

Experimental

Reagents used were Na_2CO_3 (Analar), ZrO_2 (Ventron, >99% pure), and $(NH_4)_2HPO_4$ (reagent grade). Starting materials were weighed out, ground into a paste with alcohol with an agate mortar and pestle, and dried. The mixtures were fired in open Pt crucibles in electric muffle furnaces. Decomposition was carried out at ~200 and 600 to 850°C for several hours each. Samples were then cooled, ground, and fired at ~1000°C for 2 days to complete reaction. Using this procedure, loss of soda and P_2O_5 by evaporation was negligible.

For the phase diagram work, annealing experiments were carried out on samples wrapped in Pt foil envelopes and suspended in the hot zone of a vertical tube furnace. The temperature was controlled and measured to ±3°C. At the end of each run, samples were quenched into Hg. Melting temperatures were determined approximately from the visual appearance of pelleted samples after heating at constant temperature for a few minutes.

Products of reaction and phase identification were determined using X-ray powder diffraction, with a Philips Hägg Guinier camera, Cu$K\alpha_1$ radiation. Optical microscopy using a polarizing microscope also proved useful in phase identification. For thermal analysis work three instruments were used, a Perkin–Elmer 2c DSC (20 to 450°C, heating and cooling rate 20°C/min), a Stanton Redcroft 675 DTA (up to ~1200°C, heating rate 8°C/min), and a Stanton Redcroft 780 for simultaneous DTA/TGA (heating rate 5°C/min). For accurate measurement of X-ray powder intensities and for measurement of line broadening a Philips 1020 diffractometer Cu$K\alpha$ radiation was used with a scan speed of $\frac{1}{4}°2\theta$ min^{-1} and chart speed 10 mm min^{-1}; intensities were taken as proportional to the peak areas.

Densities were measured on ~1-g samples using liquid toluene displacement pycnometry.

Results and Discussion

Na_3PO_4 Polymorphism

Our results indicate that pure Na_3PO_4 forms only two polymorphs, labeled α and γ, stable below and above ~330°C, respectively. The $\alpha \rightleftharpoons \gamma$ transition is rapidly reversible. Our conclusions are in accord with those reported by earlier workers (*3, 4, 6, 7*). We believe the so-called β polymorph (*5*) to be a hydrate or mixture of hydrates, possibly with carbonate present also. Details are as follows:

Pure, stoichiometric Na_3PO_4 was obtained by solid-state reaction of Na_2CO_3 and $(NH_4)_2HPO_4$. The $\alpha \rightleftharpoons \gamma$ transition at ~300°C was confirmed by thermal analysis. The γ polymorph could not be quenched to

TABLE Ia

X-RAY POWDER PATTERN OF PHASE(S) W

d(obs) (Å)	*I*	*d*(obs) (Å)	*I*
		2.331	35
7.026	10	2.293	50
6.624	30	2.256	20
6.422	20	2.231	20
6.261	35	2.189	50
5.850	40	2.153	30
4.599	40	2.133	30
4.475	75	2.075	55
4.314	100	2.047	35
3.701	25	2.015	40
3.519	45	2.004	50
3.392	20	1.969	30
3.355	20	1.939	20
3.296	70	1.896	30
3.195	20	1.882	30
3.118	30	1.821	30
3.083	36	1.789	20
2.922	30	1.756	40
2.879	50	1.697	20
2.847	30	1.692	20
2.803	95	1.655	10
2.717	10		
2.650	60		
2.629	40		
2.617	40		
2.579	70		
2.562	20		
2.530	10		
2.393	40		
2.366	20		

room temperature. Frequently in samples exposed to air, the α polymorph was shown to coexist with an unidentified phase(s), W, whose most intense X-ray powder lines (Table Ia) had similar *d*-spacings to the supposed β polymorph of Na_3PO_4 (5). Simultaneous DTA/TGA experiments (Fig. 1), together with ir spectroscopy, on samples containing mixtures of α and W, showed W to be a hydrated phase(s). In addition to the peak at 330°C associated with the $\alpha \rightarrow \gamma$ transition, endotherms were observed on heating at ~215 and ~255°C, both of which were accompanied by weight loss. These two peaks were not observed on the cooling cycle. On exposure of Na_3PO_4 to air for increasing periods of time, the amount of phase(s) W present increased as found by the increasing size of the DTA/TGA/DTG effects at ~215 and 255°C and by the increasing intensity of the X-ray powder lines attributed to phase(s) W.

The ir spectra of (α + W) mixtures displayed broad absorptions in the region 3000 to 3600 cm^{-1} that could be attributed to –OH stretching modes but no absorptions in the region ~1600 cm^{-1} that could be attributed to –OH bending modes. It appears that the –OH bending modes are constrained by the presence of hydrogen bonding, an effect that is to be expected from the presence of water in a structure containing PO_4^{3-} groups.

The structures of $Na_3PO_4 \cdot 0.5H_2O$ (*9*) and $Na_3PO_4 \cdot 8H_2O$ (*10*) have been reported. The X-ray powder pattern for the octahydrate was calculated using the atomic coordinates given in Ref. (*10*) and is given in Table Ib. By comparison of it and X-ray data for W, it appears that W may be a mixture of phases with probably $Na_3PO_4 \cdot 8H_2O$ as the major component.

Phase Diagram of the Orthophosphate Join, Na_3PO_4–$Na_5ZrP_3O_{12}$

The phase diagram of part of the orthophosphate join, between $Na_5ZrP_3O_{12}$ and

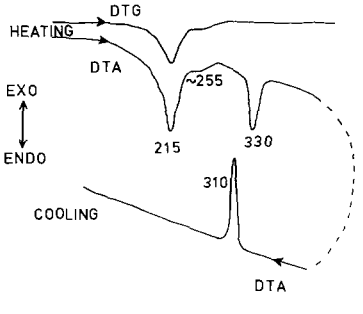

FIG. 1. Differential thermal analysis (DTA) and differential thermogravimetric analysis (DTG) traces of hydrated Na_3PO_4 phases (α + W phases).

TABLE Ib

CALCULATED X-RAY POWDER PATTERN OF $Na_3PO_4 \cdot 8H_2O$

d(calc) (Å)	I(calc)	hkl
8.451	12	100
8.026	12	020
6.504	6	$0\bar{1}1$
6.408	48	$\bar{1}30$
6.193	55	110
5.222	19	$11\bar{1}$
5.088	27	$1\bar{1}1$
4.892	7	$\bar{2}30$
4.840	52	021
4.804	31	$\bar{1}40$
4.667	11	120
4.548	36	$1\bar{3}1$
4.478	84	$\bar{2}11$
4.340	100	231
4.302	54	$12\bar{1}$
4.225	6	200
4.084	23	111
3.885	10	$\bar{1}41$
3.778	50	$\bar{1}50$
3.666	20	$2\bar{2}1$
3.665	28	$0\bar{4}1$
3.653	18	$2\bar{3}1$
3.621	17	210
3.554	9	$13\bar{1}$
3.500	38	$2\bar{1}1$
3.438	29	$\bar{1}02$
3.337	7	$\bar{3}40$
3.302	10	$11\bar{2}$
3.258	17	041
3.218	20	201
3.199	12	012
3.152	9	$\bar{2}12$
3.008	8	$1\bar{2}2$
2.926	37	$1\bar{3}2$
2.908	59	$\bar{3}60$
2.895	9	211
2.878	11	$\bar{3}01$
2.845	18	$21\bar{2}$
2.833	21	$\bar{2}42$
2,817	59	300
2.797	17	$\bar{3}61$
2.760	14	$0\bar{4}2$
2.735	31	$\bar{1}42$
2.712	26	$\bar{3}32$
2.706	12	$23\bar{1}$
2.700	38	$3\bar{2}1$
2.689	14	112
2.685	10	032
2.675	75	060
2.640	16	$\bar{3}42$

the Nasicon end member, $NaZr_2P_3O_{12}$, was reported previously (*13*); here we present data for the section Na_3PO_4–$Na_5ZrP_3O_{12}$. The orthophosphate join is not a true binary join since at melting temperatures other non-orthophosphate phases appear at certain compositions. At subsolidus temperatures, the join Na_3PO_4–$NaZr_2P_3O_{12}$ is binary however, and all the phases that appear are orthophosphates.

For the section Na_3PO_4–$Na_5ZrP_3O_{12}$, the thermal behavior of 20 compositions was studied. From the results of these experiments together with those reported earlier (*13*), the phase diagram shown in Fig. 2 was constructed. In order to make easier the comparison between different phases and solid solutions, the composition axis in Fig. 2 is given in terms of the general formula, $Na_{9-4y}Zr_y(PO_4)_3$. The end member phases Na_3PO_4 and $NaZr_2(PO_4)_3$ then correspond to $y = 0$ and 2, respectively, while for $Na_5Zr(PO_4)_3$, $y = 1$.

Na_3PO_4 forms an extensive range of solid solutions with the replacement mechanism $4Na^+ \rightleftharpoons Zr^{4+}$ and whose formula may be written as above and as shown in the lower abscissa (Fig. 2). In the report of the conductivity results, the related formula $Na_{3-4x}Zr_xPO_4$, upper abscissa, was used (*2*). The solid solution limit, y_{max}, is constant at 0.5 at low temperatures but increases somewhat at higher temperatures and has a maximum value of ~0.57 at the solidus, 1160°C. The melting temperatures of the solid solutions were determined approximately; they decrease smoothly from ~1540°C in pure Na_3PO_4 to 1160°C for $y = 0.57$.

The solid solution mechanism, $4Na^+ \rightleftharpoons Zr^{4+}$, was indicated by the results of density and lattice parameter measurements. The experimental densities of Na_3PO_4 and the solid solutions all fell in the range 2.46 to 2.62 g cm^{-3}. The lattice parameters were essentially unchanged with composition, as also is the mass of the unit cell contents, assuming the above substitution me-

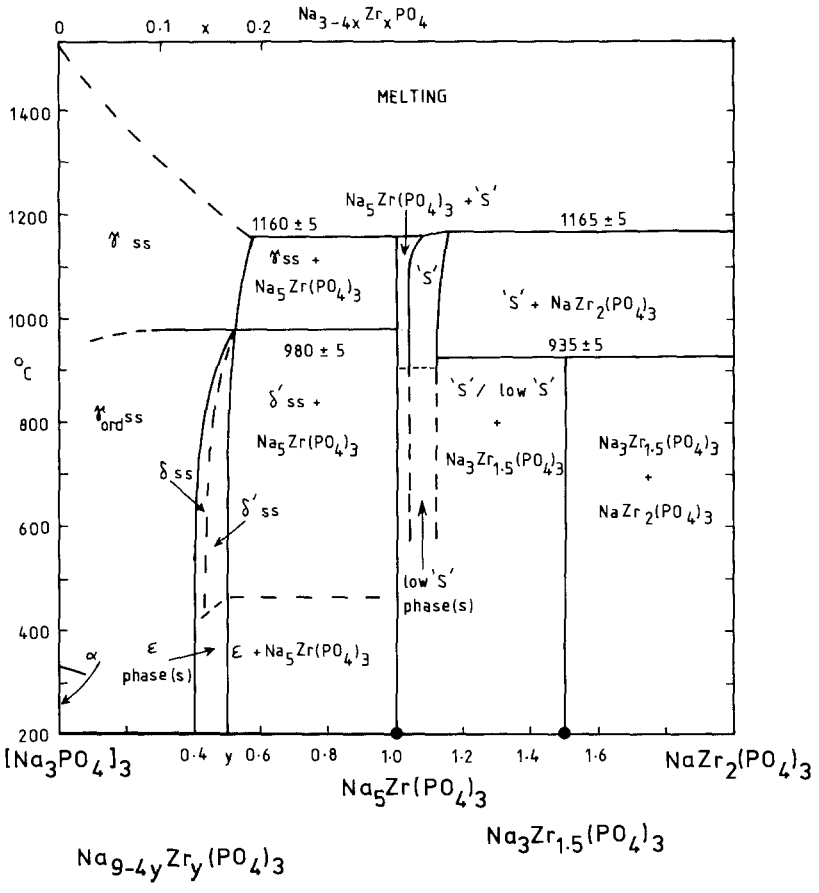

FIG. 2. Phase diagram of the orthophosphate join, Na_3PO_4–$NaZr_2(PO_4)_3$.

chanism. The calculated density of Na_3PO_4 and the solid solutions is ~2.66 g cm^{-3}. It is commonly the case that experimental density values are a few percents less than the calculated ones, due to problems associated with porosity, adsorbed gas layers, etc. Hence, the agreement between experimental and calculated densities for the present materials is regarded as being satisfactory.

The Na_3PO_4 solid solutions exhibit complex polymorphism, depending on temperature and composition. At high temperatures the cubic γ polymorph forms across the entire solid solution series, although it can be quenched to room temperature only over the range of compositions, $y \simeq 0.01$ to 0.40. For these latter compositions, the d-spacings of the X-ray powder pattern showed little variation with composition. The value calculated for a, 7.428 Å, is similar to that reported for Al-doped Na_3PO_4 (*3*).

On slow cooling and/or annealing at low temperatures for several days, the high-temperature γ solid solutions undergo various transformations, the nature of which depend on temperature and composition. The results may be summarized as follows.

For small y values $\lesssim 0.05$, mixtures of α and γ phases were generally obtained on slow cooling (~0.5 to 1°C min^{-1}) below 300°C. The range of compositions that gave

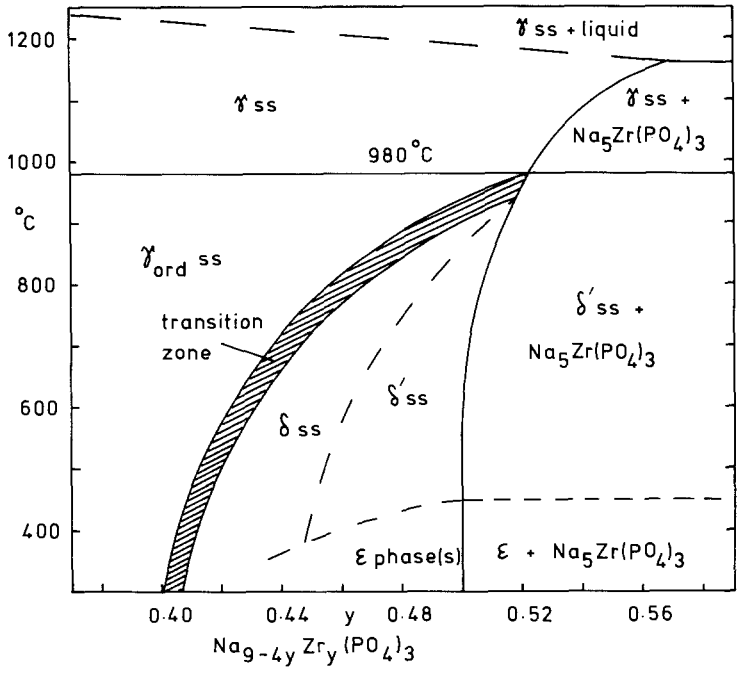

FIG. 3. Part of the phase diagram (Fig. 2) on an expanded scale.

single phase α appeared to be very limited ($y \lesssim 0.01$). For $y \gtrsim 0.0625$, no α phase was obtained.

The precise nature of the $\alpha \rightleftharpoons \gamma$ transition and its representation on the equilibrium phase diagram is not known, but some information was obtained using DSC. For pure Na_3PO_4, $y = 0$, a fairly sharp peak was observed with some hysteresis: 332°C on heating and 307°C on cooling. The hysteresis is not due to the relatively large heating and cooling rates since on slower heating (5°C min^{-1} by DTA) the peak temperature was essentially unchanged (330°C). With increasing values of y, the peaks became broader. For $y = 0.05$, a very broad peak between 250 and 330°C was observed on heating and again, with ~30°C of hysteresis on cooling. From these results it is suggested that the transition may be martensitic in nature: with increasing y, the transition takes place only partially and over an increasingly wide temperature range. For $y \gtrsim 0.0625$, no transition to α occurs and the cubic γ polymorph is observed at all temperatures. The transition is represented in Fig. 2 as a solid line that fades out for $y > 0.06$.

For larger y values, $\gtrsim 0.15$, an ordering transition occurs on cooling to give the phase labeled γ_{ord}, and for $y \gtrsim 0.40$ a structural distortion of γ_{ord} occurs to give the solid solution phases δ and δ'. The phase diagram in the region of the γ_{ord}, δ and δ' phases is shown on expanded scale in Fig. 3.

The X-ray powder pattern of γ_{ord} is shown schematically in Fig. 4b. It is characterized by two main extra lines superposed on the γ powder pattern (Fig. 4a). The powder pattern of γ_{ord} may be indexed on the basis of a face-centered cubic supercell with $a_{supercell} = 2a_{subcell}$ (Table II). Optically the γ_{ord} phase is isotropic; however, in view of the limited number of supercell reflections, single crystal studies are needed

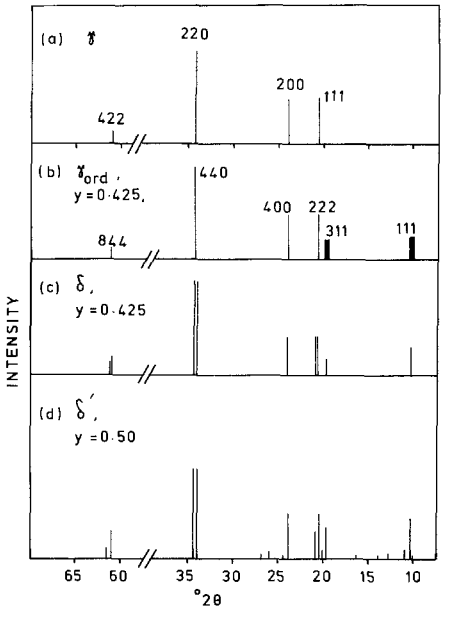

FIG. 4. Schematic X-ray line diagrams. Samples (b), (c), and (d) were prepared by quenching from 800, 600, and 600°C, respectively.

in order to confirm the unit cell of γ_{ord}.

The supercell lines of γ_{ord} were generally broader than the subcell lines, as indicated in Fig. 4b. It was found that they could be sharpened by annealing at progressively lower temperatures, particularly for the larger y values, approaching $y = 0.40$. However, even for the composition $y = 0.40$, the line broadening was not eliminated by prolonged annealing for 30 days at 400°C.

Formation of the δ phase was shown by the splitting into doublets of several lines in the γ_{ord} pattern (Fig. 4c). This occurred for compositions with $y > 0.40$ and the degree of splitting increased with increasing y. By measuring the degree of splitting for several compositions and extrapolating to zero line splitting, a lower limiting value of $y \simeq 0.40$ was found for the δ phase.

Within the δ phase field, $y \gtrsim 0.40$, further complexities were observed. For $y \gtrsim 0.45$, an additional set of weak lines appeared in the X-ray powder pattern (Fig. 4d). When this occurred, the phase was labeled δ′. In addition, for $y \gtrsim 0.45$, prolonged annealing below ~450°C lead to decomposition/transformation of the δ/δ′ phase to give unidentified products with a complex X-ray powder pattern. These have been labeled the ε phase(s).

A DTA endotherm was observed at high temperatures for all Na_3PO_4 solid solution compositions with $y \gtrsim 0.12$. The temperature of the endotherm increased slightly from 960°C for $y = 0.12$ to a fairly constant 980°C for $y > 0.25$. The size of the endotherm increased with y. Hence for $y < 0.12$, it either did not exist or was too small to be detected. Various pieces of experimental evidence, discussed later, indicate that this reversible DTA effect is associated with the transition $\gamma_{ord} \rightleftarrows \gamma$.

The phase $Na_7Zr_{0.5}(PO_4)_3$ that has been reported very recently (*14*) corresponds to the low-temperature limit, $y = 0.50$, of the

TABLE II

X-RAY POWDER DIFFRACTION DATA FOR γ_{ord}, $y = 0.4$

d obs (Å)	*I*	*d* calc (Å)	*hkl*
8.623	25	8.577	111
4.499	20	4.479	113
4.300	50	4.289	222
3.722	40	3.714	400
2.629	100	2.626	044
2.145	10	2.144	444
1.858	25	1.857	008
1.517	15	1.516	448
1.314	10	1.313	088

Note. Cubic unit cell dimensions: $a(\gamma_{ord}) = 2a(\gamma) = 14.856$ Å. Sample annealed at 400°C for 30 days. KCl internal standard added. A weak line at 2.861 Å is presumed to be due to a hydrated phase, but may possibly conceal a very weak 333, 511 supercell line, $d_{calc} = 2.859$ Å. This line is attributed to a hydrate phase since its intensity varies from sample to sample, it does not show the characteristic peak profile of γ_{ord} supercell lines and it is not a γ line.

Na_3PO_4 solid solution series. The powder pattern reported for this is essentially that of γ_{ord} (Table II), with one extra reflection at 2.859 Å; interestingly it has been indexed on the basis of a hexagonal unit cell. Our phase diagram studies show that the composition $y = 0.5$ can be prepared in at least three forms at room temperature, viz. as γ_{ord} by quenching from $\gtrsim$980°C, as δ/δ' by quenching from temperatures in the range ~500 to 980°C, and as ε by prolonged annealing at, e.g., 400°C.

Domain Size Measurements and Order–Disorder Effects

In order to understand better the order–disorder transition $\gamma_{ord} \rightleftharpoons \gamma$ and to clarify the phase diagram in the region $y = 0.40$ to 0.50, samples of five different compositions, $y = 0.40$, 0.425, 0.45, 0.475, and 0.50, were subjected to isothermal annealing at several temperatures on a stepwise heating cycle. For the compositions $y = 0.40$, 0.45, and 0.50, annealing was commenced at 600°C and terminated at 1030°C with temperature increments of 40 to 100°C. At the end of each isothermal anneal, samples were quenched into Hg and analyzed by X-ray powder diffractometry, with a slow scan speed, $\frac{1}{4}°2\theta$ min^{-1}. The sample was then returned to the furnace for the next annealing. Thus, for each composition, the same sample was used throughout the stepwise annealing cycle. It was assumed that equilibrium had been reached at a particular temperature when no changes occurred on further annealing at the same temperature. The time taken to reach equilibrium varied from 11 days to 4 hr, depending on temperature. A further check that equilibrium had been reached was carried out by subjecting one composition, $y = 0.45$, to a stepwise cooling cycle, commencing at 1030°C. The results were generally the same as those found on the heating cycle.

Using the above experiments, the following features were studied as a function of temperature and/or composition: (i) the breadth and area of the 111, 113 supercell peaks in γ_{ord} for $y = 0.40$ and the corresponding peaks in δ,δ' for $y \geq 0.425$; (ii) the degree of splitting of the lines characteristic of the δ,δ' phases, in particular using the lines at ~61°2θ (Fig. 4); (iii) the additional weak extra lines that characterize the δ' phase.

Since the same set of samples was used throughout, it was not possible to add an internal standard. However, the supercell peak 400 of the γ_{ord} pattern (i.e., the 200 subcell peak) at 23.9°2θ (Fig. 4b), was found to be a suitable internal standard since it did not exhibit broadening or splitting under any conditions. Further, its net intensity was effectively independent of temperature, as shown by a separate set of experiments in which weighed amounts of KCl were added to samples of $y = 0.45$ that had been annealed at 600°C (to give phase δ) and 930°C (to give γ_{ord}). The intensity of the peak at 23.9°2θ in these two samples was found to be the same to within ±3%.

The broadening of the supercell lines in the γ_{ord} phase, attributed to the presence of small ordered domains, was quantified using the Warren–Scherrer formulae

$$B^2 = B_B^2 - B_s^2$$

$$t = \frac{0.9\lambda}{B \cos \theta}$$

in which B_B, B_s are the widths in radians, at half peak height, of the broadened line and a standard, unbroadened line of similar 2θ value, respectively. t is the domain diameter, λ the X-ray wavelength, and θ the Bragg angle for the broadened line. In this work, as described above, the internal standard was the 200 subcell line at 23.9°2θ (i.e., the 400 supercell line).

The results of these various experiments may be summarized as

—The line broadening associated with the

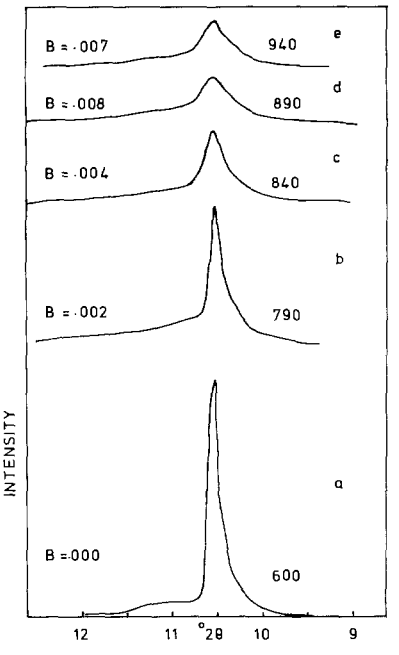

FIG. 5. Variation in shape of the supercell peak at 10.4°2θ for samples quenched from the temperatures shown for composition $y = 0.45$.

supercell peaks, characteristic of the γ_{ord} phase, is attributed to the presence of small domains of ordered structure.

—In the γ_{ord} field, the domain size decreases with (a) increasing temperature up to a limit of ~980°C and (b) decreasing y.

—The intensity (area) of the supercell peaks decreases with decreasing y but is essentially independent of temperature for a given y.

—The transition $\delta \rightarrow \gamma_{ord}$ takes place over a range of temperatures (~50°C). This transition zone is characterized by (a) a reduction in the degree of line splitting that occurs in the δ phase and (b) the onset of broadening of the supercell lines.

—The transition $\gamma \rightarrow \gamma_{ord}$, on cooling, takes place extremely rapidly. For compositions $y \gtrsim 0.4$ the γ phase cannot be quenched to room temperature. The transition $\gamma \rightarrow \gamma_{ord}$ takes place in two stages: rapid growth of a large number of small domains, followed by domain growth and a reduction in the number of domains. The first of these processes occurs extremely rapidly during quenching and cannot be avoided with the quenching rates used.

The experimental results on which these conclusions are based are:

For the line broadening and domain size measurements, the 111 supercell line at 10.4°2θ was used. This is shown for one composition, $y = 0.45$, at five different temperatures in Fig. 5. Three effects are apparent in the results. (1) At low temperatures, composition $y = 0.45$ has the δ structure in which no significant line broadening occurs (Fig. 5a). (2) At higher temperatures, in the γ_{ord} field, line broadening occurs which increases with increasing temperature (Figs. 5b to d). (3) At the highest temperatures >850 to 900°C (Fig. 5d, e) the line broadening in the quenched samples is essentially independent of temperature provided that the samples are quenched rapidly.

From results such as these domain sizes were determined. These are plotted against composition for one temperature, 840°C, in Fig. 6 and against temperature for composition $y = 0.45$ in Fig. 7a. The results for compositions $y = 0.4$ and 0.5 are plotted

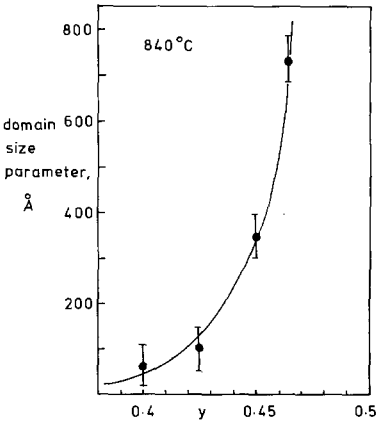

FIG. 6. Variation of domain size parameter, t, with composition for samples quenched from 840°C.

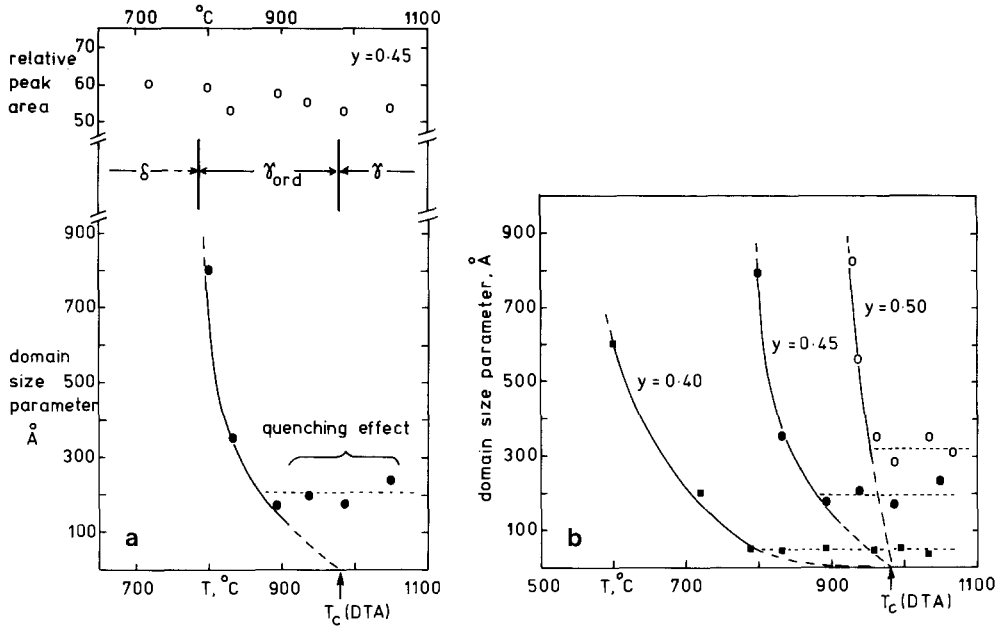

FIG. 7. (a) Variation of domain size parameter and area of 10.4°2θ peak with temperature for y = 0.45. (b) Variation of domain size parameter with temperature for three different compositions.

together with y = 0.45 in Fig. 7b. Also shown in Fig. 7a is the variation in relative area of the 111 supercell peak as a function of temperature for y = 0.45; results for compositions y = 0.4 and 0.5 (not shown) were similar.

The results of Figs. 6 and 7 together show that the broad supercell peaks associated with small domain size are characteristic of the γ_{ord} phase (Fig. 3); in the δ,δ' phases, no significant broadening was observed. As the boundary of the δ field is approached, from within the γ_{ord} field, domain sizes increase increasingly rapidly, either by increasing y for a given temperature (Fig. 6) or decreasing the temperature for a given composition (Fig. 7). However, although for a given composition the domain size decreases with increasing temperature, the total intensity of the supercell lines and hence the total amount of material within the ordered domains is independent of temperature and is essentially unchanged through the $\gamma_{ord} \rightleftharpoons \delta$ transition (Fig. 7). This means that a relatively small number of large domains, at low temperatures, is breaking up in a reversible manner, to give an increasingly large number of smaller and smaller domains with rising temperature. For each composition, this process is observed over a range of temperatures; it is seen most clearly in Fig. 7 for composition y = 0.45 over the temperature range 800 to 900°C.

At still higher temperatures, e.g., >900°C for y = 0.45, the ordered domains become very small and appear to be surrounded by disordered material. During quenching, the domains then grow in size by consuming the disordered material until the domains impinge upon each other. This is the explanation for the approximate constancy in domain size above a certain temperature (~800°C, y = 0.40; ~950°C, y = 0.50).

The disordering process and reduction in domain size is presumed to be complete by ~980°C, the temperature of the endotherm

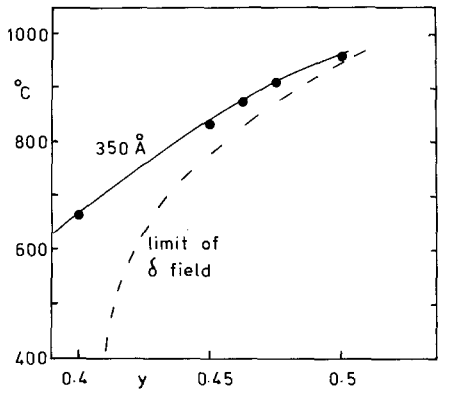

FIG. 8. Variation of temperature with composition for a given domain size parameter, 350 Å. Dashed line represents the upper temperature/lower y limit of the δ phase field.

observed on DTA for these γ_{ord}, δ,δ' compositions.

The variation of domain size with temperature and composition is further emphasized by plotting temperature against composition for a given domain size, as shown in Fig. 8 for domain size of 350 Å.

The variation in relative intensity (area) of the 10.4°2θ supercell peak as a function of composition is shown in Fig. 9. This shows clearly the reduction in overall order at small y values.

Discussion

Although we have no direct structural information on the Na_3PO_4 solid solutions

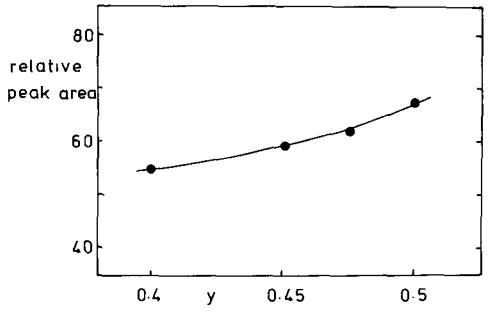

FIG. 9. Variation of relative intensity of the supercell peak at 10.4° 2θ with composition y.

formed by partial replacement of sodium by zirconium a neutron diffraction study on related $Na_{3-3x}Al_xPO_4$ solid solutions has been reported (*7*). The Na_3PO_4 structure has been described as essentially a cation excess, antifluorite structure. Its formula may be written as

$$Na^{int}[Na_2PO_4]$$

in which the unit in square brackets represents the antifluorite structure with Na^+ cations occupying, ideally, the eightfold positions $\frac{1}{4}, \frac{1}{4}, \frac{1}{4}$, etc. and PO_4^{3-} anions occupying corner and face center positions. The extra Na^+ ions, Na^{int}, occupy the interstitial sites at the cube body center and edge centers.

In the $Na_{3-3x}Al_xPO_4$ solid solutions, it was found that the sodium vacancies were largely distributed over the Na^{int} sites. If we assume that the zirconium-based solid solutions are similar, their formula may be written

$$Na^{int}_{3-4y}Zr^{int}_{y}[Na_2PO_4]_3.$$

The upper limit for this replacement mechanism would correspond to $y = 0.75$ whereas, in fact the maximum extent of solid solution was found to be rather less, $y = 0.50$ at low temperatures, rising to $y \sim 0.56$ at 1150°C.

The unit cell of γ-Na_3PO_4 and the γ solid solutions contains 4 formula units and the composition $y = 0.375$ corresponds to the situation in which each unit cell contains, on average, 0.5 Zr^{4+} ions. One possible cause of the $2 \times 2 \times 2$ ordering of cubic subcells in the cubic γ_{ord} phase may therefore be that alternate cubic subcells contain 0 and 1 zirconium ions in ordered fashion. This would give an "ideal" composition of $y = 0.375$ for the γ_{ord} phase, which fits in reasonably well with the experimental observation that the γ_{ord} phase has a limiting composition at low temperatures of $y \simeq 0.4$; for larger y, the δ,δ' phases form. In addition, the supercell lines characteristic of the

γ_{ord} phase are most intense and showed the least line broadening at low temperatures for composition $y = 0.40$.

This hypothesis also accounts, qualitatively, for the decrease in domain size with decreasing y: for $y < 0.375$, a fully ordered structure is not possible and either the total mass of the fully ordered domains must decrease, giving a mixture of ordered domains of composition $y = 0.375$ and disordered regions of smaller y, or all the material is involved in domain formation but there is considerable disorder within the individual domains. The experimental results tend to support the first of these two possibilities.

An additional ordering mechanism must be invoked to explain the formation of δ,δ' phases at larger y, and especially, the formation of δ' with an apparent ideal composition of $y = 0.50$. At this composition, half of the interstitial sites would be occupied on average. This could be a random process involving Na^+, Zr^{4+} ions disordered over alternate interstitial sites. Alternatively, it could involve a more complex ordering of Na^+, Zr^{4+} ions and vacancies since at this composition, $y = 0.50$, two in every three cubic subcells would contain, on average one Zr^{4+} ion. The formula given above for the solid solutions assumes that the Zr^{4+} ions occupy the interstitial sites. An additional possibility or complication is that these may instead replace Na^+ ions in the $[Na_2PO_4]$ antifluorite-like component of the structure in such a way that the Zr^{4+} ions are concentrated in these sites whereas the cation vacancies are associated with the interstitial sites.

In summary, we propose the following model for the Na_3PO_4 solid solutions. At high temperatures, the cation vacancies, caused by the replacement mechanism $4Na^+ \rightleftharpoons Zr^{4+}$, are disordered over the Na^{int} sites in the γ phase. The Zr^{4+} ions may be either in these same sites or may form part of the antifluorite-like "framework." With increasing y at low temperatures, the Zr^{4+} ions first begin to order themselves in alternate cubes, leading to the γ_{ord} phase with a cubic supercell and a domain structure. The domains have ideal composition, $y = 0.375$. For $y > 0.375$, additional ordering processes come into effect and a second "ideal" composition occurs at $y = 0.50$. This may involve Zr^{4+} ions ordered in two of every three subcells or a more complex mechanism involving Zr^{4+}, Na^+ ions, and vacancies. In this region, the structure is slightly distorted from cubic pseudosymmetry.

Acknowledgments

We thank the SERC for a research studentship (S. J. M.) and a research grant (A. R. W.).

References

1. S. J. MILNE, PhD. thesis, University of Aberdeen (1984).
2. S. J. MILNE AND A. R. WEST, *Mater. Res. Bull.* **19,** 705 (1984).
3. M. PALAZZI AND F. RÉMY, *Bull. Soc. Chim. Fr.* **8,** 2795 (1971).
4. J. M. NEWSAM, A. K. CHEETHAM, AND B. C. TOFIELD, *Solid State Ionics* **1,** 377 (1980).
5. M. KIZILYALLI AND A. J. E. WELCH, *J. Inorg. Nucl. Chem.* **38,** 1237 (1976).
6. A-W. KOLSI, *Rev. Chim. Miner* **13,** 416 (1976).
7. J. M. NEWSAM, A. K. CHEETHAM, AND B. C. TOFIELD, *Solid State Ionics* **1,** 395 (1980).
8. E. TILLMANNS AND W. H. BAUR, *Inorg. Chem.* **9,** 1957 (1970).
9. M. T. AVERBUCH-POUCHOT AND A. DURIF, *J. Solid State Chem.* **46,** 193 (1983).
10. L. LARBOT AND J. DURAND, *Acta Crystallogr. Sect. C* **39,** 12 (1983).
11. A. HOOPER, P. MCGEEHIN, K. T. HARRISON, AND B. C. TOFIELD, *J. Solid State Chem.* **24,** 265 (1978).
12. S. J. MILNE, J. A. GARD AND A. R. WEST, *J. Mater. Sci. Lett.* **2,** 680 (1983).
13. S. J. MILNE AND A. R. WEST, *Solid State Ionics* **9/10,** 865 (1983).
14. A. CLEARFIELD, R. GUERRA, A. OSHARSSON, M. A. SUBRAMANIAN, AND W. WANG, *Mater. Res. Bull.* **18,** 1561 (1983).